Journal of Food Engineering 359 (2023) 111697

Contents lists available at ScienceDirect

Journal of Food Engineering

journal homepage: www.elsevier.com/locate/jfoodeng

Digital twins for monitoring and predicting the cooking of food products: A case study for a French crêpe

Iulen Cabeza-Gil [a,*,1], Itziar Ríos-Ruiz [a,1], Miguel Ángel Martínez [a,b,1], Begoña Calvo [a,b,1], Jorge Grasa [a,b,1]

[a] Aragón Institute of Engineering Research (i3A), University of Zaragoza, Spain
[b] Centro de Investigación Biomédica en Red en Bioingenieria, Biomateriales y Nanomedicina (CIBER-BBN), Spain

ARTICLE INFO

Keywords:
Digital twins
Domestic appliances
Smart cooking
Neural networks
Cooking
Frying pan
Food processing

ABSTRACT

The food industry is shifting toward automated and customized processes, leading to the emergence of smart cooking devices that improve cooking outcomes. However, these devices can be invasive, costly, and only applicable to certain foods. To address these issues, a noninvasive digital twin that monitors food during cooking using a common frying pan with a temperature sensor and a weighing scale is proposed. A case study for a French crêpe is presented, in which we developed a digital twin using a neural network trained on over 400,000 simulation data points. The results show that the digital twin can accurately estimate the properties of the crêpe during cooking in real time with a mean absolute percentage error of less than 5% and predict when it will be cooked according to user criteria. The approach offers significant benefits over existing smart cooking devices, as it can be applied to a wide range of cooking processes. The proposed technology enables food process automation and has potential applications in both home and professional kitchens.

1. Introduction

New technologies, such as artificial intelligence (AI) and the Internet of Things (IoT), are being developed in the food processing sector to enhance food quality, safety, and flavor (Khouryieh, 2021; Knorr and Augustin, 2021). Among these technologies, the use of digital twins (DTs) is one of the most promising and involves the virtual representation of a physical system to reproduce complex processes in real time and provide valuable information, ultimately leading to the best decision-making (Defraeye et al., 2021; Verboven et al., 2020; Khan et al., 2022). With the aid of new devices, such as IoT sensors that connect the DT and the physical system in real time, production lines and products themselves can be improved (Kaur et al., 2019).

In pursuit of achieving desirable attributes in food products, the study of flavors and aromas is becoming increasingly essential for the production of new foods (such as 3D printing or cell cultivation), as well as the cooking process itself (Nachal et al., 2019; Mishyna et al., 2020; Zhang et al., 2021). Two popular trends in cooking are the use of AI for recipe creation and the use of DTs to monitor the state of food being cooked in real time (Wang et al., 2019). The latter is of special interest, as it can account for the variability caused by the human–system interaction during cooking (Aguilera, 2018; Dolejšová et al., 2020).

Recent studies have demonstrated the use of DTs to monitor the cooking processes of ice cream machines (Karadeniz et al., 2019), food in convection ovens (Kannapinn and Schäfer, 2021), and chicken fillets (Kannapinn et al., 2022). This work aims to develop a DT to monitor the cooking process of food in a frying pan on an induction hob, demonstrating that representative food properties, such as temperature, color, and weight loss, can be accurately monitored using a temperature sensor in the pan and a weighing scale in the hob. The proposed technology is particularized to the frying of a French crêpe (Fig. 1) in a pan heated by a smart induction hob, which can control the pan temperature according to a control algorithm (Cabeza-Gil et al., 2020a). With this DT, the cooking process of the French crêpe can be estimated in real time and forecast in advance, enabling the user to make informed decisions during the cooking process and paving the way for a fully autonomous cooking kitchen.

In contrast to prior studies that utilized reduced-order models (ROMs) for digital twin development (Kannapinn and Schäfer, 2021; Kannapinn et al., 2022), this work proposes a digital twin architecture based on deep neural networks (DNNs). The neural network is trained with a vast amount of data (over 400,000 samples) obtained from high-fidelity simulations using the finite element method (FEM). While

* Correspondence to: Edificio Betancourt, Universidad de Zaragoza, Calle María de Luna, 3, 50018 Zaragoza, Spain.
E-mail address: iulen@unizar.es (I. Cabeza-Gil).

[1] Financial Disclosure: No author has a financial or proprietary interest in any material or method mentioned.

https://doi.org/10.1016/j.jfoodeng.2023.111697
Received 15 October 2022; Received in revised form 15 August 2023; Accepted 16 August 2023
Available online 18 August 2023

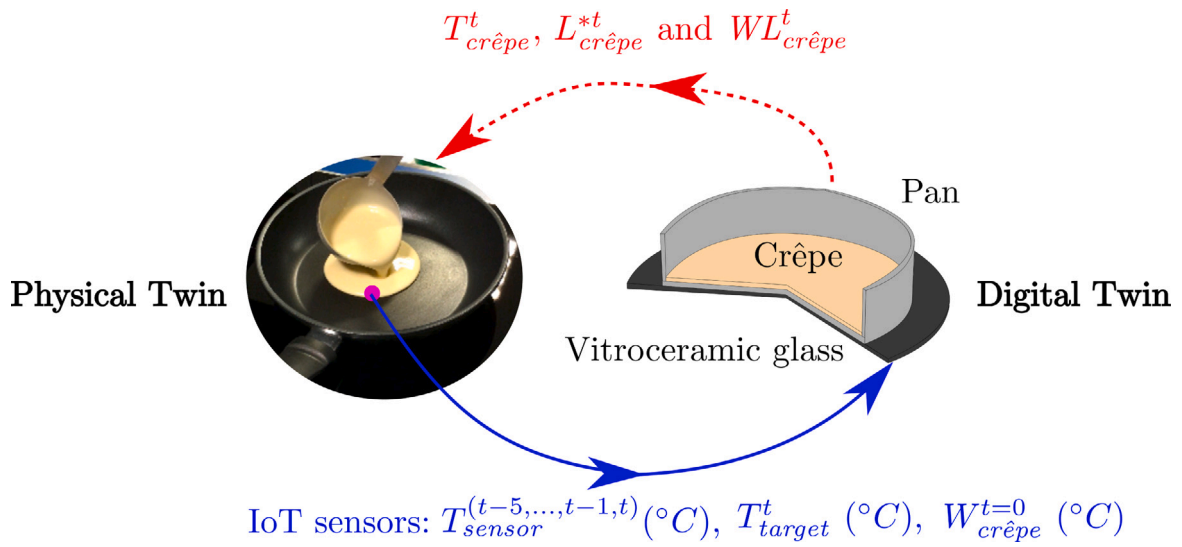

Fig. 1. DT for assisted cooking. The physical twin is connected to the DT through IoT sensors: the temperature sensor placed in the pan ($T^{(t-5,\ldots,t-1,t)}_{sensor}$, pink circle), the initial weight of the batter ($W^{t=0}_{crêpe}$), and the target temperature of the pan provided by the user in the smart cooking hob (T^t_{target}). With these data, the virtual model can provide the crêpe state in real time (the temperature and color on both sides and the weight loss, $T^t_{crêpe}$, $L^{*t}_{crêpe}$ and $WL^t_{crêpe}$, respectively).

ROMs require less computational capacity and ensure that the physical principles govern the digital twin's predictions, the combination of neural networks and FEM might provide more accurate predictions in complex scenarios and unusual cases.

2. Methods

The digital twin developed here can replicate the cooking process of a French crêpe. By using data from IoT sensors, it can monitor cooking parameters from the physical twin, such as the temperature of the frying pan and the weight of the batter. Based on this information, the system can calculate in real time several parameters that describe the state of the crêpe, including its temperature, color, and weight loss (as shown in Fig. 1). This allows the system to provide information about the doneness of the food and estimate when it should be turned over or removed from the pan.

In this section, the development process of the digital twin is outlined, covering its inception through to its final architecture and operation. The first step involves elucidating the mathematical model for cooking a French crêpe on a smart induction cooktop. This model provides the groundwork for creating high-fidelity simulations, achieved through the numerical resolution of the mathematical model using FEM. Following this, the strategy for generating large amounts of in silico data to train the neural network is discussed, and these data are subsequently utilized to train the neural network. Finally, the DT architecture, which is essentially a neural network, and its functionality are comprehensively described.

2.1. Mathematical model for the cooking of a French crêpe

The cooking of the crêpe was modeled as a coupled transient heat and mass transfer problem, where the batter was heated by contact with the hot surface of a pan. The mathematical model involved several simplifying assumptions: an axisymmetric representation of the geometry and heating flux power was used; only energy and mass transport mechanisms were considered, with the assumption that the crêpe batter was reasonably viscous; the thickness was very low and no gas phase overpressure was assumed, avoiding the need to account for any change of momentum of the batter bulk; the pan was heated by an inward heating flux, and heat was transferred to the batter with a very high thermal contact conductance; the heat was transferred to the batter by conduction and convection from the air, which constituted the heat loss mechanism in the external surface; liquid water diffused within the crêpe batter, and local evaporation occurred simultaneously; water and water vapor transport were considered separately as multiphase transport species, and the water vapor generated in the crêpe batter migrated to the top surface and diffused into the environment; the thermal contact conductance drastically decreased as a crust formed on the bottom of the batter in contact with the pan when the viscosity increased.

In this section, the key equations that define the crêpe cooking model are presented. For a more comprehensive description of this model, the reader is referred to Lorente-Bailo et al. (2021). The equation that governs the heat transfer mechanism in the aluminum pan is:

$$P + k_{pan}\nabla^2 T = \rho c_e \frac{\partial T}{\partial t} \tag{1}$$

where P is the volumetric power density generated by induction, k_{pan} is the thermal conductivity, ρ is the density and c_e is the specific heat of the pan material.

Inside the crêpe, considering the water energy absorption during evaporation:

$$\nabla \cdot \left(k_{\text{crêpe}} \nabla T\right) = \rho_{\text{crêpe}} C_{\text{crêpe}} \frac{\partial T}{\partial t} + Q_{evp} \tag{2}$$

where the evolution of the crêpe heat conductivity is a function of batter porosity ε, water content per unit of dry mass X_l, air heat conductivity λ_{air} and the parameters a and b:

$$k_{\text{crêpe}} = \left(a\frac{X_l}{1+X_l} + b\right) \frac{(1-\varepsilon)\left(2\left(a\frac{X_l}{1+X_l}+b\right)+\lambda_{air}\right)+3\varepsilon\lambda_{air}}{(1-\varepsilon)\left(2\left(a\frac{X_l}{1+X_l}+b\right)+\lambda_{air}\right)+3\varepsilon\left(a\frac{X_l}{1+X_l}+b\right)} \tag{3}$$

For batters made of wheat flour, $a = 0.8026$ W/(m·K) and $b = 0.8374$ W/(m·K) were selected (Lorente-Bailo et al., 2021). The density and specific heat of the crêpe were calculated considering the density and specific heat of the batter constituents and the solid, liquid and vapor mass fractions (x_s, x_l and x_v):

$$\rho_{\text{crêpe}} = \frac{1}{\frac{x_s}{\rho_s}+\frac{x_l}{\rho_l}+\frac{x_v}{\rho_v}} \qquad C_{\text{crêpe}} = x_s C_s + x_l C_l + x_v C_v \tag{4}$$

The term Q_{evp} represents the energy absorbed by the water during the evaporation process:

$$Q_{evp} = \rho_p \sigma_{evp} f_v L_{evp} \tag{5}$$

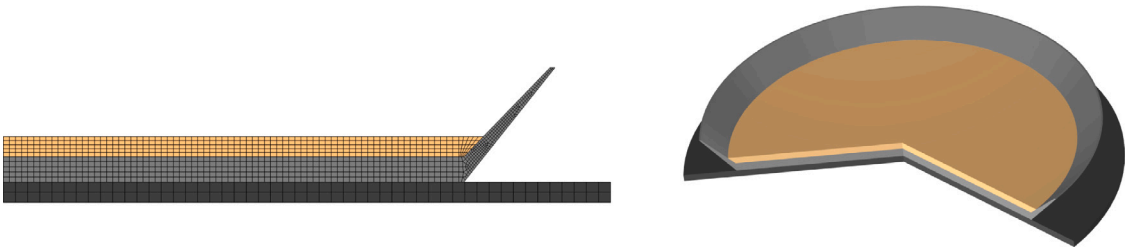

Fig. 2. Two-dimensional axisymmetric finite element mesh and 3D view representation of the three domains.

where σ_{evp} is an evaporation rate constant, L_{evp} is the water latent heat of vaporization, and f_v is an empirical normalized function:

$$f_v = \begin{cases} exp\left(-\left(\frac{T-T_{\eta_{max}}}{\xi}\right)^2\right), & T \leq T_{\eta_{max}} \\ 1, & T > T_{\eta_{max}} \end{cases} \quad (6)$$

where $T_{\eta_{max}} = 74.7$ °C and $\xi = 3.33$ °C.

The relations that govern the diffusion of the liquid and vapor phases inside the product are:

$$\frac{\partial x_l}{\partial t} = \nabla\left(D_l \nabla x_l\right) - \sigma_{evp} f_v, \qquad \frac{\partial x_v}{\partial t} = \nabla\left(D_v \nabla x_v\right) + \sigma_{evp} f_v \quad (7)$$

where $x_s + x_l + x_v = 1$ is the constraint. $D_l = 4.3337 \cdot 10^{-10}$ m^2/s and $D_v = 9.6599 \cdot 10^{-8}$ m^2/s are the water and vapor diffusion coefficients, respectively, and $\sigma_{evp} = 5.1623 \cdot 10^{-4}$ s^{-1} is the rate of water evaporation. The empirical conductivity and evaporation constants were obtained from an optimization fitting performed at our previous research comparing numerical and experimental data (Lorente-Bailo et al., 2021).

2.1.1. Boundary conditions

An initial uniform temperature of 20 °C was considered for all the parts of the model, the glass, the pan and the crêpe. All external surfaces of the cooking system had convection heat losses (h_{glass}, h_{pan}, $h_{\text{crêpe}}$) and only the pan was considered to have radiation losses (e). A $h_{\text{crêpe}}$ of 14.5 W/(m^2· K) was considered. The remaining terms were varied according to the design of experiments conducted shown in Section 2.3.

Moreover, a mass flow of vapor was incorporated in the top surface of the crêpe according to:

$$-D_v \nabla x_v = k_v \rho_{\text{crêpe}} (x_v - x_{v_a}) \quad (8)$$

where x_{v_a} is the humidity of the surrounding air governed by the following equation:

$$x_{v_a} = x'_{v_a} \frac{\rho_a}{\rho_{\text{crêpe}}} \quad (9)$$

where x'_{v_a} is the vapor fraction and ρ_a is the air density at ambient temperature.

To model the thermal interaction between the crêpe and the pan, a thermal contact conductance was considered as:

$$h_c^{\text{crêpe}}(t) = h_{c0}^{\text{crêpe}}(1.05 - f_v) \quad (10)$$

where $h_{c0}^{\text{crêpe}} = 1905$ W/(m^2· K). The thermal interaction between the pan and glass was modeled with a thermal contact conductance, h_c. Its value throughout the batch of simulations is discussed in Section 2.3.

2.2. Computational model and the finite element mesh

An axisymmetric computational model was developed to reproduce the cooking process in COMSOL Multiphysics® v.5.2a. The model consisted of three different domains, as shown in Fig. 2. The vitroceramic glass had a thickness of 4 mm, the aluminum pan had an internal diameter of 180 mm and a thickness of 5 mm, and the lateral wall was 50 mm in height. The crêpe diameter was identical to the interior diameter of the pan and had variable thickness depending on the mass considered by the user. The selected discretization consisted of 1118 quadrilateral elements and 1393 nodes using a quadratic approximation for both the mass and heat transfer. Automatic time increments were taken by the implicit backward differentiation method, and solution outcomes were saved every 1 s. The power-density field acting in the pan via the induction hob was implemented using a distribution determined experimentally as in Sanz-Serrano et al. (2017). Since this power depends on the target temperature chosen, the smart cooking system supplies power until the target temperature is reached. This was achieved by controlling the power supplied by a PI algorithm with the temperature sensor in the pan (see Fig. 1). To implement this power control in COMSOL, an ordinary differential equation (ODE) was used in the domain defined by the bottom surface of the pan. The target temperature was randomly chosen in every simulation and could vary randomly throughout cooking.

2.2.1. State of the crêpe

The solution provided by the model allows us to establish the cooking state of the crêpe, defined in this case by the following variables: temperature of the batter throughout the cooking process (calculated for all the nodes of the FEM, Fig. 3), evolution of weight loss as a result of evaporation, and evolution of the color on both sides of the product.

The weight loss percentage (WL) of the crêpe was calculated as follows:

$$\text{WL}(t) = \left(1 - \frac{\int_V \rho_{\text{crêpe}}(t) dV}{\int_V \rho_{\text{crêpe}_0} dV}\right) \cdot 100 \quad (11)$$

where $\rho_{\text{crêpe}_0}$ is the initial crêpe density and $\rho_{\text{crêpe}}(t)$ is the actual density.

Browning is the result of a combination of Maillard reactions and caramelization (Ame, 1992). A browning model can be defined by first-order kinetics with the browning rate depending on the temperature and the water content (Sanz-Serrano et al., 2017). The evaluation of the progress of browning can be conveniently carried out by the lightness parameter L^* of the standard color space CIE $L^*a^*b^*$:

$$L^*_{\text{crêpe}}(r,z) = -\left(k_1 + \frac{k_2}{x_l}\right) e^{\left(-\frac{A_1 + \frac{A_2}{x_l}}{T(r,z)}\right)} \quad (12)$$

where $T(r,z)$ is the temperature in the crêpe domain. The parameters dependent on the water content, $k_1 = 15.4$, s^{-1}, $k_2 = 2.22 \cdot 10^{-14}$ s^{-1}, $A_1 = 3.22 \cdot 10^{-14}$ K and $A_2 = 2240$ K, were fitted from experimental data.

2.3. In-silico dataset acquisition

A machine learning methodology, specifically a DNN, has been stated as the base for the DT. DNNs need large amounts of data to be defined reliably. The main problem with these approaches usually comes from the acquisition of these training data. The ideal approach is to use experimental data. However, numerical models often replace it for two reasons: the capability to provide essential data that cannot be

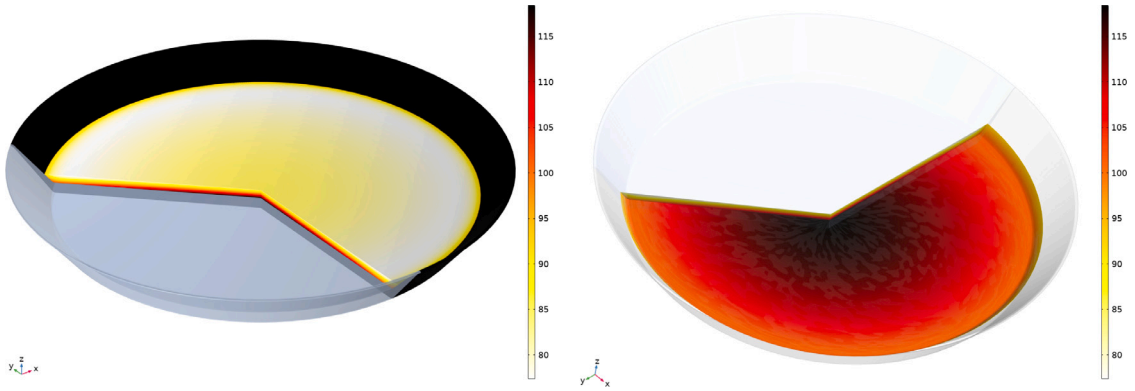

Fig. 3. Model outcome for one of the cooking simulations where 3D representations of the temperature (^{o}C) distribution are shown on both sides of the crêpe just before the turn over.

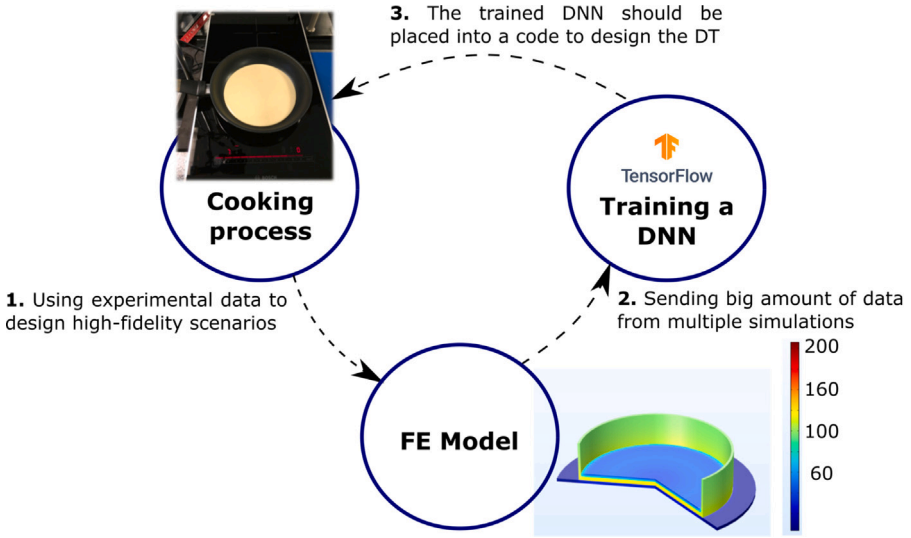

Fig. 4. Experimental data is used to validate the FE model. The FE model creates multiple high-fidelity scenarios that are used to train a DNN. Last, the trained DNN is programmed in the DT to elucidate aspects of the ongoing cooking process in real-time.

physically measured (Defraeye et al., 2021) (in this work, the color and temperature of the side of the crêpe in contact with the pan) and, above all, the possibility to provide a considerably larger dataset. Thus, the data needed to design a usable DNN for this purpose were obtained via high-fidelity simulations of the cooking of a French crêpe (Cabeza-Gil et al., 2020a; Lorente-Bailo et al., 2021; Bonet-Sánchez et al., 2022) as described in Section 2.1. The results provided by the model constitute the dataset used to train the DNN that will predict the cooking process in real time for the DT, as described in Fig. 4.

Different cooking scenarios were simulated considering, on the one hand, the variability introduced by the user and, on the other hand, the heat transfer parameters related to different pan characteristics (Table 1). During preparation, it was considered that the user could add an amount of batter between 90.8 and 136.2 g during the first 90 s after turning on the induction cooktop. The target temperature range of the smart cooktop was between 120 and 220 °C and was randomly changed throughout the cooking process, simulating possible interactions between the user and the induction hob. This means that the user can set the cookware surface temperature between that range at all times. The simulations also considered the cooking time for each surface of the batter, which lasted from 30 to 90 s.

To account for different geometries and construction materials of the pan, Table 1 shows the ranges of thermal properties and loss coefficients for the conduction, convection and radiation mechanisms that pans might present. A large number of possible scenarios of the cooking process were generated by randomly varying the coefficients for the boundary conditions of the glass and the pan, as well as the thermal conductance, in each simulation according to the ranges provided in Table 1.

A total of 4490 different computational models were simulated using a Latin hypercube sampling method. Fig. 5 summarizes the wide variety of cooking simulations performed by describing a representative scenario. As shown in this figure, the cooking was discretized in time steps of one second ($\Delta t = 1s$), and the simulation ended when the crêpe was turned out (after cooking the second crêpe side).

2.4. Architecture of the deep neural network

The DNN was trained with the aim of estimating the system state (crêpe and pan) at the following time step (t+1). As previously mentioned, the crêpe state is defined by its average temperature ($T_{crêpe}$) and color ($L^{*}_{crêpe}$) on both sides and the weight loss it experiences during the cooking process ($WL_{crêpe}$).

A total of 3349 (88%) of the 4490 simulated cooking processes were used to train and validate the DNN, while the remaining 541 (12%) cooking simulations were used in the testing phase. Since a sample rate of 1 s was chosen, and the final cooking time for each simulation was randomly chosen, a training dataset of 399,318 different cooking states was obtained.

Table 1
Range of the parameter variation for the heat transfer properties of the pan and heat transfer mechanisms at the model contours (Bonet-Sánchez et al., 2022).

Intrinsic properties of the pan			Loss coefficients			
Density ρ [Kg m^{-3}]	Specific heat c_e [J g^{-1} K^{-1}]	Conductivity k [W m^{-1} K^{-1}]	Pan convective coef. h_{pan} [W m^{-2} K^{-1}]	Glass convective coef. h_{glass} [W m^{-2} K^{-1}]	Thermal contact conductance h_c [W m^{-2} K^{-1}]	Pan emissivity e [-]
7800	[300–450]	[50–220]	[3–9]	[3–9]	[50–100]	[0.5–1]

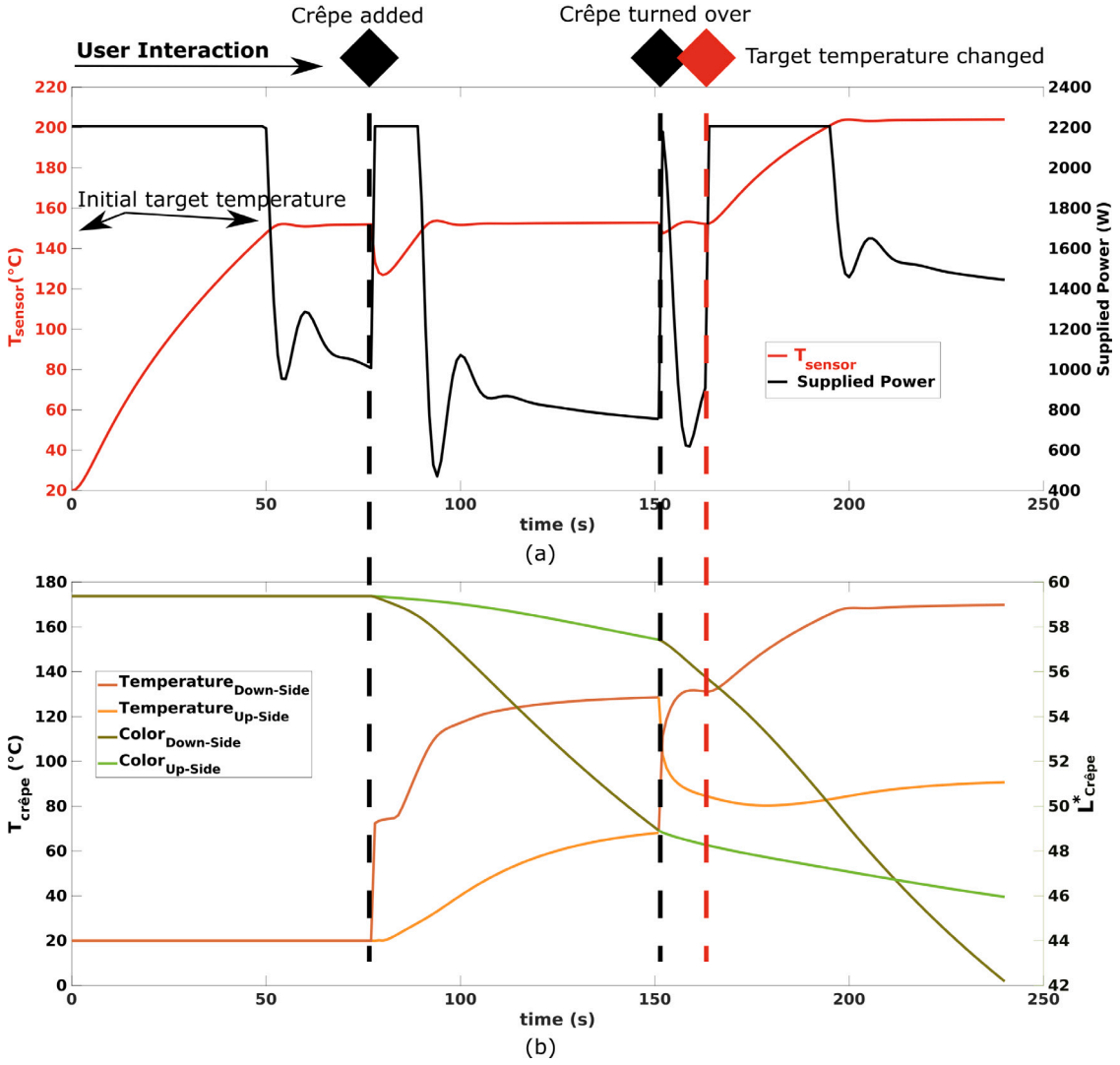

Fig. 5. Example of a cooking simulation in an induction system with PI control. (a) shows the temperature of the pan sensor and the power applied, and (b) shows the surface average temperature ($T_{crêpe}$) and color of the crêpe ($L^*_{crêpe}$). The temperature target level was set to 150 °C. The crêpe was added 80 s after the beginning of cooking, when the pan temperature had reached the initial target temperature. Adding the crêpe implies a temperature drop of 20 °C in the pan. Then, the underside of the crêpe was cooked 70 s before it was flipped . Right after, the temperature target level was increased from 150 °C to 200 °C at 165 s, simulating a possible interaction of the user with the induction hob. Note that the down side of the crêpe is always in contact with the pan; thus, it changes when the crêpe is turned over.

The DNN was customized as follows. The widely used rectified linear unit (ReLU) was selected as the activation function (Ramachandran et al., 2018) since the ReLU function overcomes the vanishing gradient problem, allowing models to learn faster and perform better (Moolayil, 2019). The chosen optimization method was the Adam function (Kingma and Ba, 2014), as it has shown good performance in the training of DNNs. The selected loss function, which will guide the neural network in its training, was the mean squared error (MSE). The root mean squared error (RMSE) and mean absolute percentage error (MAPE) were also used as metrics:

$$\mathrm{MSE} = \frac{1}{n}\sum_{i=1}^{n}(\boldsymbol{y} - \hat{\boldsymbol{y}})^2 \tag{13}$$

$$\mathrm{RMSE} = \frac{1}{n}\sum_{i=1}^{n}\sqrt{(\boldsymbol{y} - \hat{\boldsymbol{y}})^2}, \tag{14}$$

$$\mathrm{MAPE} = \frac{1}{n}\sum_{i=1}^{n}\frac{\|\boldsymbol{y} - \hat{\boldsymbol{y}}\|}{\boldsymbol{y}} \tag{15}$$

where n is the number of samples, $\boldsymbol{y}$ is the ground-truth value and $\hat{\boldsymbol{y}}$ is the predicted response. MSE is an interesting metric because it overexposes the presence of outliers in the predictions and is recommended when the error distribution is expected to be Gaussian (Chai and Draxler, 2014).

Finally, two additional functions to improve the performance of the DNN were included: (i) a function that reduces the learning rate when there has not been a decrease in the loss function (MSE) in 10 epochs

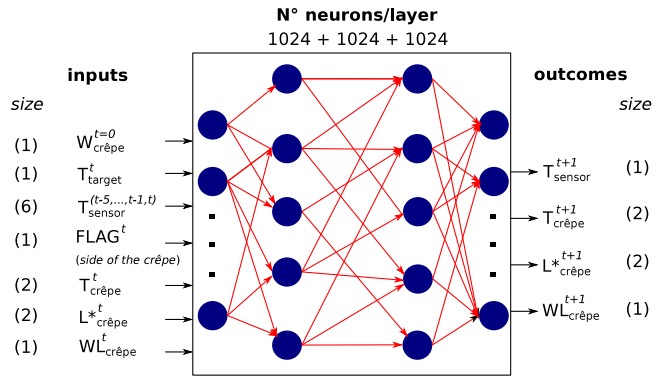

Fig. 6. DNN architecture. The final network consists of three hidden layers with 1024 neurons each, a total of 7 inputs and 4 output variables.

and (ii) an early stopping at 50 epochs if the loss function does not decrease at an established rate without reaching the total number of epochs initially determined. This last function is important in terms of computational training cost. A batch size of 32 was used, which is the number of samples processed at once during training and before an update of the parameters of the network. DNN training was performed in Keras (Chollet et al., 2015) and resulted in an average training time of 4 h and 30 min using a commercially available GPU (GeForce GTX 2060 SUPER).

A sensitivity analysis as in Cabeza-Gil et al. (2020b) was performed to define the simplest neural network possible to best predict the results. To achieve this, the following procedure to find the optimal DNN was conducted. Initially, a DNN with three hidden layers of 256 neurons each was trained. Subsequent iterations doubled the number of neurons per layer until the MSE did not decrease. The final architecture configuration is shown in Fig. 6.

2.5. Development of the digital twin

The design of the DT is meant for an executable at the device level. The executable contains a trained DNN that uses as input the information measured by the IoT sensors in the physical system and provides as output the virtual representation of the problem. For the purpose and validity of this work, the DT is a set of Python code that contains the trained DNN. Since the overall aim is to provide information about a cooking process, the sampling rate of these sensors was established at 1 Hz for data acquisition, a sufficient frequency to make informed decisions while cooking and to perform calculations by the integrated algorithm in real time. The same rate was used to estimate the crêpe state.

The overall structure and architecture of the DT is presented in Fig. 7, according to the estimation and forecasting functionalities. The input variables of the DT, which are provided by the IoT sensors (Fig. 7.a), include the initial weight of the batter $W^{t=0}_{crêpe}$, the target temperature of the pan established by the user T^{t}_{target}, and an event detection input ($FLAG^{t}$) that indicates the turn over of the crêpe and the pan sensor temperature at the current and five previous seconds $T^{(t-5,\ldots,t-1,t)}_{sensor}$. These are also inputs for the DNN that runs below the DT, as well as other internal inputs that are fed backward from previous iterations of the DNN, as shown in the green lines in Fig. 7.b, such as the average temperature of the crêpe in the bottom and upper surfaces $T^{t}_{crêpe}$, the average color of the crêpe in both surfaces based on the lightness value of the CIELAB color space $L^{*t}_{crêpe}$ and the weight loss due to water evaporation $WL^{t}_{crêpe}$. The crêpe temperature and color are averaged due to both the high homogeneity in the surfaces and to reduce model parameters.

2.6. Digital twin functionality

The DT developed in this study can estimate and even forecast different parameters of the cooking process that define the state of the crêpe in the pan, which in this study have been defined as the temperature and color of the food on both sides and the weight loss (see Fig. 1). These three parameters could be subsequently used to determine the degree of doneness of the food and establish their value when the crêpe required turning over or was fully cooked. The **estimation functionality** of the DT consists of determining these parameters in the current instant, considering the temperature of the pan and other inputs. The **forecast functionality** entails predicting the outcome of the cooking process as long as no further action is taken by the user, which is to say, the DT can predict when the crêpe will be properly cooked. Both actions are achieved through a deep neural network (DNN) that feeds on the data provided in real time by the IoT sensors: a temperature sensor in the pan, the temperature target level imposed by the user in a smart induction hob and the initial weight of the added food (Fig. 7). The estimation of the state of the crêpe (temperature, color and weight loss) is performed with the real pan temperature obtained directly from the sensor at the specific instant, as well as the five previously measured temperatures. These measurements are also used to predict the temperature of the pan in the following instant for the forecast. By inputting the pan temperature in several timepoints, the system can predict the characteristics of the cooking system (i.e., the pan characteristics (k, h_c) including heat losses (h_{pan}, e)). This temperature will be an input for a new iteration, and following this procedure in a loop, the final state (moment when the degree of doneness customized by the user is achieved) of the crêpe will eventually be obtained.

When using the **estimation functionality** of the DT, the output or estimated data is the state of the crêpe at the current instant. In fact, at the instant immediately after (t+1)–, i.e., the average temperature of the crêpe $T^{t+1}_{crêpe}$, its average color $L^{*t+1}_{crêpe}$ and weight loss $WL^{t+1}_{crêpe}$. These parameters and the estimated temperature of the pan sensor T^{t+1}_{sensor} are also outputs of the DNN. Note that with these estimations, the DT is able to monitor the color and consequently the degree of doneness even for the hidden surface of the crêpe. As can be observed in Fig. 7.a, the output variables that define the state of the food ($T^{t+1}_{crêpe}$, $L^{*t+1}_{crêpe}$ and $WL^{t+1}_{crêpe}$) are used subsequently as inputs of the DNN to calculate the next step of the process.

When performing the **forecast functionality**, the DT can also anticipate the evolution of the cooking process and provide the user some useful information, such as when to turn over or remove the crêpe to avoid a burned side. This is inferred from the output parameters commented on previously but predicted in the future after several loop iterations of the system. These iterations involving future values of variables can be performed with the DNN estimation of the pan sensor temperature in the next instant T^{t+1}_{sensor} (see blue lines in Fig. 7.b). With this predicted temperature and the variables that characterize the state of the crêpe fed as new inputs, and after several internal iterations of the DNN, a forecast of the whole cooking process can be performed. This prediction will be valid provided that the user does not perform any modifications in the cooking, such as turning over the crêpe or changing the target temperature. If any of those actions were taken, the prediction would be updated by the DT.

3. Results

3.1. Model results

The performance of the DT has been evaluated with the testing dataset. A total of 541 cooking scenarios were obtained from FE simulations that are completely new to the system. This means that the target temperature, the initial weight of the batter and the temperature of the pan of each of these scenarios were introduced as inputs, as

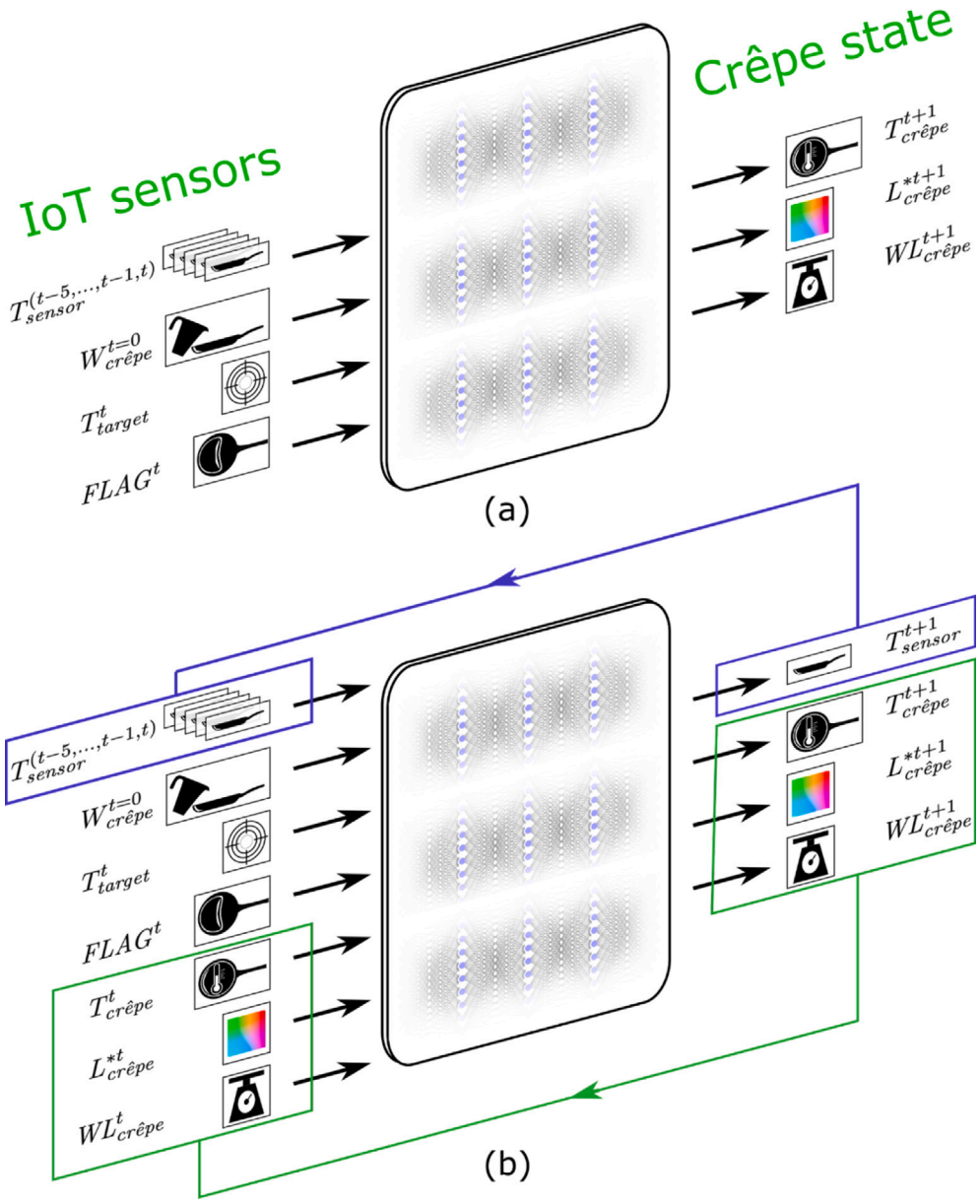

Fig. 7. Schematic outline (a) and architecture (b) of the DT. (a) The DT is able to provide information of the state of the crêpe only with the information provided by the IoT sensors. (b) Internal functioning of the DT. The information provided by the IoT sensors is complemented by three internal inputs related to the state of the crêpe in the measuring instant. These internal inputs are fed backward from the system (see green line). This loop is performed in both the estimation and forecast, as the information related to the state of the crêpe cannot come from the sensors. T^{t+1}_{sensor} is only relevant and fed backward (blue line) for the forecast functionality, while the estimation functionality is derived from the physical sensor in the pan.

these would be the data provided by the IoT sensors in the real cooking process. With these inputs, the DT performs the **estimation** in real time for each time period ($\Delta t = 1s$) and the **forecast** of the state of the crêpe, and these results are subsequently compared with the simulated outcome with the metrics defined in Section 2.4. Moreover, the effect of the possible noise in the measurements taken in the real situation is quantified and evaluated at the end of this section.

3.2. Estimation in real-time

Table 2 shows the RMSE and MAPE of the 541 cooking scenarios used for testing. The RMSE and MAPE of the crêpe state (temperature, color and weight loss) were calculated once the batter was poured into the pan for each simulation. The mean of all simulations was calculated and is shown in Table 2 with the standard deviation. A relative error below 5% is achieved for all responses, implying that the DT can provide physical estimations in real time with high accuracy. As an illustrative example of the cooking process, Fig. 8 shows the estimated and ground-truth values for a representative cooking scenario. Both present significant agreement during the whole cooking process. The weight loss of the crêpe differs slightly for long cooking times.

3.3. Cooking forecast

Table 3 shows the RMSE and MAPE of the forecast values of the 541 cooking scenarios. The variables related to the state of the crêpe were evaluated once the crêpe was added to the pan, whereas the temperature of the pan sensor was predicted from the beginning of cooking. As could be expected, the forecast response presents higher errors than the estimation in real time, as this functionality is based on the iteratively estimated temperature of the pan for future time intervals. Fig. 9 shows an example of the forecast throughout a certain

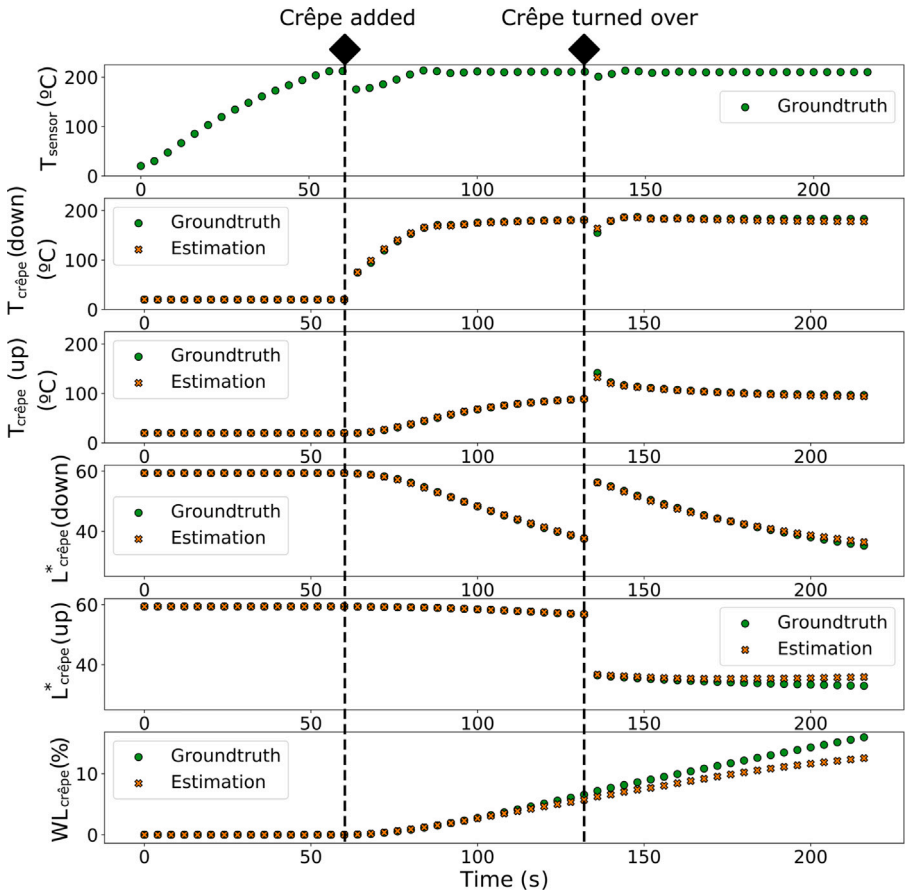

Fig. 8. Example cooking scenario and real-time estimation of double-sided crêpe cooking. The state of the crêpe is only known at the start of cooking as initial conditions. All estimations of the state of the crêpe are performed based on the estimation in the previous increment, as well as on data from the sensors. Note that "*down*" refers to the crêpe side in contact with the pan, while "*up*" refers to the visible side. Thus, when the crêpe is turned over, the temperature of the opposite face is measured.

Table 2
Mean and standard deviation of the real-time estimation error metrics in the 541 cooking simulations. The proper estimation is evaluated using the RMSE and MAPE. The MAPE of the weight loss is not calculated due to the amount of times the ground truth for this variable takes the value of zero.

	$T_{\text{crêpe}}(down)$	$T_{\text{crêpe}}(up)$	$L^*_{\text{crêpe}}(down)$	$L^*_{\text{crêpe}}(up)$	$WL_{\text{crêpe}}$
RMSE	5.86 ± 1.41 (°C)	4.79 ± 1.41 (°C)	1.03 ± 0.52 L	0.89 ± 0.53 L	1.07 ± 0.57 (%)
MAPE	4.32 ± 1.27 (%)	2.83 ± 0.90 (%)	1.21 ± 0.77 (%)	0.66 ± 0.65 (%)	–

Table 3
Mean and standard deviation of the forecast error metrics in the 541 cooking simulations. Same as in the estimation functionality, the MAPE of the weight loss is not calculated due to the amount of times the ground truth for this variable takes the value of zero.

	T_{sensor}	$T_{\text{crêpe}}(down)$	$T_{\text{crêpe}}(up)$	$L^*_{\text{crêpe}}(down)$	$L^*_{\text{crêpe}}(up)$	$WL_{\text{crêpe}}$
RMSE	9.68 ± 12.37 (°C)	9.07 ± 5.08 (°C)	5.21 ± 1.44 (°C)	1.11 ± 0.51 L	0.92 ± 0.59 L	1.07 ± 0.57 (%)
MAPE	4.68 ± 6.32 (%)	6.65 ± 3.55 (%)	3.69 ± 1.74 (%)	1.31 ± 0.75 (%)	0.72 ± 0.64 (%)	–

cooking scenario. The forecast temperature of the bottom side of the crêpe is less accurate than the estimated temperature shown in the previous section, as can also be seen in Table 3. This is expected for the forecasting functionality, as the temperature of the sensor is estimated for future times instead of working with the actual value measured in real time by the IoT sensor, similar to the estimation functionality. As can be observed in Fig. 9, the longer the period of DT prediction is, the greater the error.

3.4. Evaluation of the effect of noise measurements by the IoT sensors in DT estimation

In the study, two different evaluations of the sensors were carried out. Initially, to assess the effect and relevance of each IoT sensor in the estimation of the cooking process, the value of each sensor was randomly introduced in the system (see Table 4, lines #1, #2 and #3). With this new random value, the estimated results, in terms of the color of the down and up sides of the crêpe, were compared with values reported in Section 3.2 (Table 4, line #0). If the new results do not differ notably from the original values, the effect of the measurements provided by that sensor in particular would be negligible for the DT. This evaluation was performed as a sensitivity analysis to verify that all IoT sensors are necessary for the DT of the cooking process. Out of the three values measured by the IoT sensors, only the target temperature seems to not have a meaningful effect on the estimated response of the DT (see Table 4). This parameter does not affect the real-time estimation, as the temperature of the system cannot drastically change immediately after a variation in the target temperature. Therefore, no parameters of the state of the crêpe vary significantly in 1 s even with an abrupt change in the target temperature. This measure is, however,

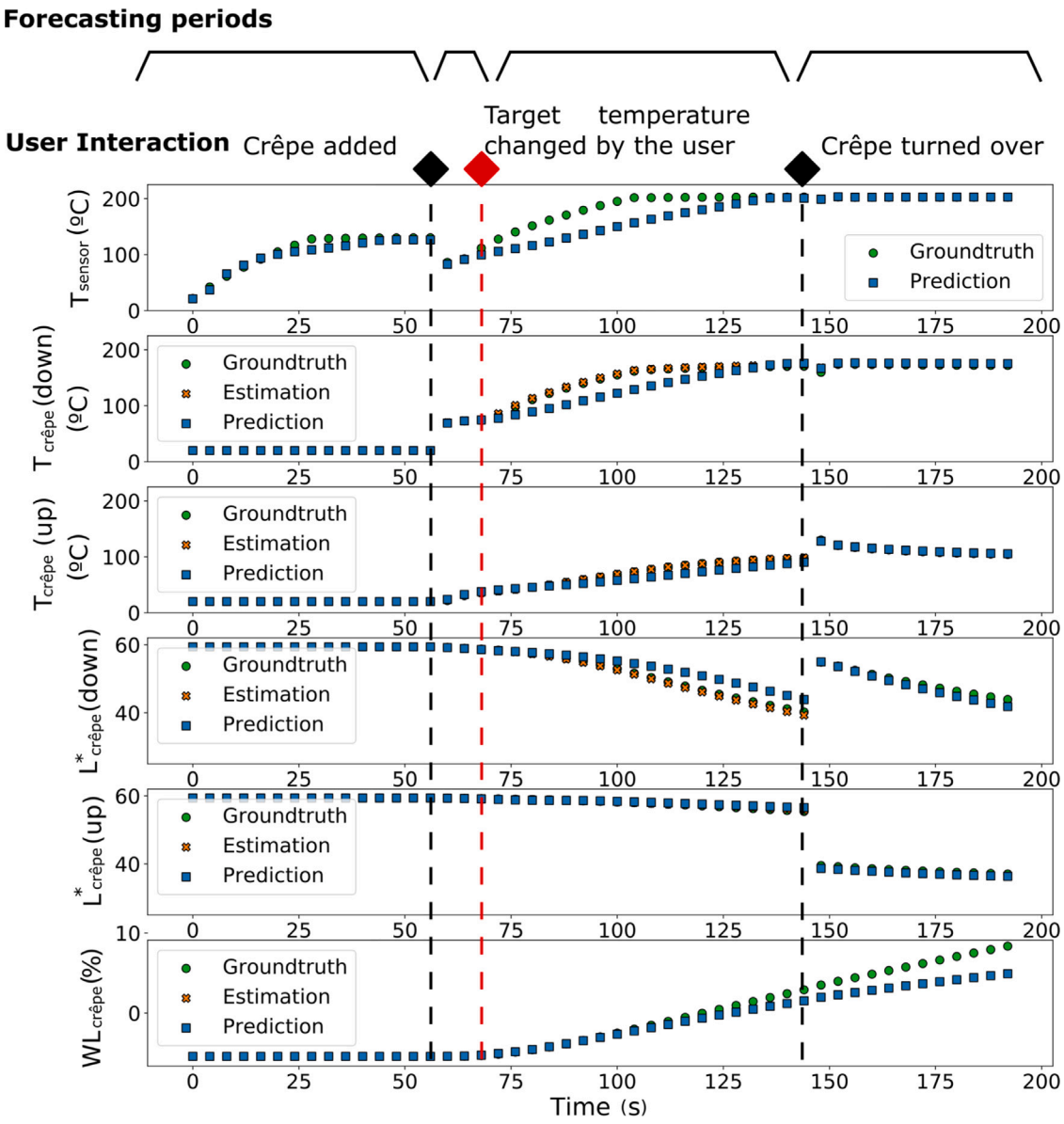

Fig. 9. Example of forecasting crêpe cooking. The DT performs its forecast during periods when external actions are not performed in the system, as shown above the graphs. The first forecast involves the beginning of the cooking up to 55 s, when the crêpe is added. From this moment, the DT forecasts the variables up to 65 s, where the target temperature was changed. Then, it forecasts until the crêpe is turned around (t=145 s). Finally, the crêpe was removed at 190 s. Note that in the real application, the DT would give a forecast for a long period (i.e., 200 s), but the forecast of the DT would be updated once a perturbation was performed (e.g., a change in the target temperature or adding the crêpe). In the weight loss of the crêpe, the estimation values cannot be seen, as they lie right below the prediction values.

crucial for forecasting the cooking process, as it leads the temperature of the system in the long term.

After that, the effect of possible noisy measurements typical of experimental situations was tested (see Table 4, lines #4, #5 and #6). For that purpose, different scenarios considering different deviations in the temperature pan sensor and the initial batter weight were evaluated. Speckle noise was added. The results obtained show that the error due to noisy variations in the measurements of the sensors is notably low in all cases lower than 1.4%.

4. Discussion

The main goal of this research was to develop a noninvasive DT that could estimate and forecast food properties during cooking. Although the method was particularized to the cooking of a double-sided crêpe as a proof-of-concept, it could be applied to different types of food in a domestic induction hob using other common vessels. The DT allows us to know the main features that characterize the state of the crêpe (temperature, color and weight loss) during and in advance of the cooking process with a MAPE less than 4.32 ± 1.27% in temperature and 1.21 ± 0.77% for the color on both sides of the crêpe in the estimation functionality. For the forecasting functionality, a temperature and color MAPE less than 6.65 ± 3.55% and 3.69 ± 1.74%, respectively, were obtained.

The biggest potential of this technology against other nonconnected approaches that do not use IoT sensors (and thus are not connected in real-time to the physical inputs) is the capability of instantaneously responding to any possible user interaction (e.g., adding the crêpe or changing the target temperature). Another advantage of the method is that it works for any pan that lies in the range of the characterizing variables simulated (Table 1), provided that a temperature sensor is placed on the cookware surface, with no need to input or even know the specific pan characteristics.

The results showed that the DT can elucidate physical aspects of the ongoing process with a high accuracy (a relative error below 5%),

Table 4
MAPE of the estimation of the color of both sides of the crêpe in the sensitivity analysis of the IoT sensors (lines #1, #2 and #3) and when the inputs of the sensors are varied randomly simulating noisy or erroneous measurements (lines #4, #5 and #6).

	Physical input	Variability range	MAPE $L^*_{\text{crêpe}}(down)$ (%)	MAPE $L^*_{\text{crêpe}}(up)$ (%)
#0	–	–	1.21 ± 0.76	0.66 ± 0.65
#1	Target temperature	Totally random	1.39 ± 0.09	0.98 ± 1.11
#2	Temperature pan sensor	Totally random	∞	∞
#3	Initial batter weight	Totally random	∞	∞
#4	Temperature pan sensor	$[-2.5, 2.5]$ °C	1.23 ± 0.82	0.73 ± 0.69
#5	Initial batter weight	$[-10, 10]$ g	1.33 ± 0.76	0.77 ± 0.67
#6	Temperature pan sensor – Initial batter weight	$[-2.5, 2.5]$ g–°C	1.24 ± 0.77	0.71 ± 0.63

as can be observed in Table 2. As expected, the forecast results were slightly less accurate than the estimated values in real time (see Table 3). However, the most unfavorable situation was evaluated, where the prediction was performed only once at the beginning of the process or when a change was introduced in the system. In the real situation, the prediction could be performed and updated as many times as the designer wants, improving the accuracy while moving forward in the cooking process.

These results showed that a DNN can be accurately trained to reproduce the FE model results in real time (t<1 ms, the amount of time taken to update the estimation by the DT), considering only the information provided by the IoT sensors (temperature of the pan sensor and weight of the crêpe). Moreover, if the FE model is properly validated, the outputs of the DNN and thus of the DT can be accepted as valid for the physical cooking system. With the novelty of forecasting included in this study, the variables of interest (crêpe state) can be quantified over time only by knowing its initial state. The critical point of this technology is to develop a realistic FE model since the validity of the dataset depends on it. As long as there are high-fidelity simulations (Moya et al., 2021), the DT will provide accurate data. Furthermore, this particular study could not be performed with only experimental data, as the color and temperature of the crêpe side in contact with the base pan can only be currently quantified through numerical methods.

Reviewing the other study in the literature, Kannapinn and Schäfer (2021) obtained an RMSE of less than one degree in the microwave cooking process. However, the authors performed a different approach to build their DT, formulating a hybrid physics-based data-driven DT framework, whereas this DT is based on a DNN trained with the data obtained from an FE model that combines two validated models (Lorente-Bailo et al., 2021; Cabeza-Gil et al., 2020a). The data-driven approach intrinsically takes into account the physics of the problem, while the trained DNN can resemble a black box. However, the DNN has two distinct advantages: i) By definition, all kinds of complex physical relations are considered between the outputs and inputs; ii) all possible scenarios can be introduced and trained in the DNN, assuring that the DNN will be robust against any unpredictable event.

Contrary to other implementations in the market (e.g., the smart grilling hub Weber Connect (Weber-Stephen Products LLC, USA)), which requires a temperature sensor in the cooked food, the proposed technology is noninvasive and thus does not alter the food properties. Moreover, this is a fixed installation and avoids the need for the user to set up the device. This technology could be implemented for cooking different types of food (vegetables, soup, meat) in different cooking appliances if properly validated FE models are created. The implementation of this system could change domestic cooking, as different actions could be carried out based on AI.

The main limitation of this study is its theoretical approach. Although the variability inherent to experimental measurements in the IoT sensors was considered (Section 3.4), the manufacturer should consider the speed and quality of data collection and other unimaginable events that occur in real situations that could lead to inaccurate DT predictions. One solution for this problem could be the addition of some physical controllers in the input and output of the DT to filter outliers and ensure that the input physically makes sense. Moreover, the crêpe state was considered to be defined by the temperature, color and weight loss. There are other parameters that could be added to the model to customize the degree of doneness, such as the texture (tenderness) for meat DT solutions. However, numerical models simulating these effects are still in an early stage of development.

Finally, we utilized the average temperatures of the crêpe as key markers. To enhance the construction of an augmented reality cooking model across the entire spectrum, it is possible to explore more refined architectures like convolutional neural networks. These architectures could effectively extract variables within the whole domain.

5. Conclusions

A smart cooking technology based on digital twins that provides information on the state of food in real time and in advance was developed. This noninvasive system uses the information provided by IoT sensors and is thus suitable for use in smart kitchens. The cooking of a double-sided French crêpe in an induction hob was used as a proof of concept. Nonetheless, there is a wide range of possible applications as long as high-fidelity simulations of different cooking processes are developed.

CRediT authorship contribution statement

Iulen Cabeza-Gil: Conceptualization, Methodology, Validation, Writing – original draft. **Itziar Ríos-Ruiz:** Methodology, Validation, Writing – original draft. **Miguel Ángel Martínez:** Writing – review & editing, Supervision, Project administration, Funding acquisition. **Begoña Calvo:** Writing – review & editing, Resources, Supervision, Funding acquisition. **Jorge Grasa:** Software, Validation, Writing – review & editing, Supervision.

Declaration of competing interest

None. No author has a financial or proprietary interest in any material or method mentioned.

Data availability

Data will be made available on request.

Acknowledgments

This work was funded through project CPP2021-008938 HIPATIA financed by MCIN/AEI/10.13039/501100011033 (Spanish Ministry of Science and Innovation), and by the European Union NextGenerationEU/PRTR; and by BSH Home Appliances Group. It was also supported by the Department of Industry and Innovation (Government of Aragon) through the research group Grants T24-23R and T07-23R. I. Cabeza-Gil also acknowledges research support from NextGenerationEU (Margarita Salas).

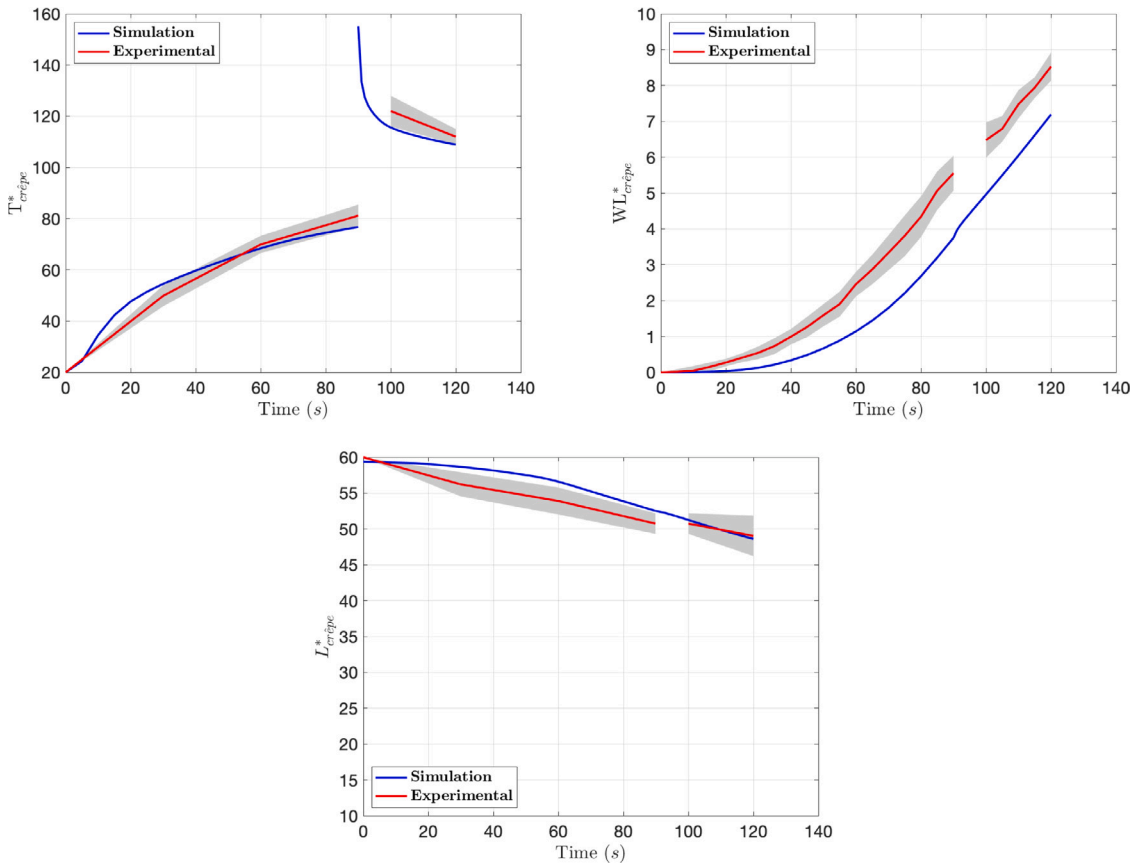

Fig. 10. Experimental results of the average surface temperature ($T^*_{crêpe}$), weight loss ($WL^*_{crêpe}$) and color ($L^*_{crêpe}$). The experimental data shown are the mean (±) standard deviation of five replicates..

Appendix. Model validation

The set of parameters that were used in the model to develop the DT were obtained from a previous work (Lorente-Bailo et al., 2021) where only one side of the crêpe was cooked. Since the results presented in this study involved cooking both sides, a validation of the computational model is presented briefly in this section.

A series of cooking tests ($n = 5$) were performed using crêpe batter (wheat flour, 26.77% w/w, whole milk 51.63% w/w, pasteurized hen egg 21.03% w/w and salt 0.57% w/w) and a forged aluminum 180 mm diameter and 5 mm thickness pan with a thin bottom steel layer and a nonstick coating (Easy Induction, Kuhn Rikon, Zell, Switzerland). The crêpes were cooked for 90 s and then turned over to complete a total cooking time of 120 s. The crêpe weight loss during the process was monitored by placing the hob on a balance (DS30K0.1L, Kern & Sohn, Balinger-Frommern, Germany) with 0.1 g precision that records data every 1 s. During the cooking period, a thermographic image of the upper side of the crêpe was taken at 30 s intervals, and the radial temperature profiles were determined using the software Testo IRsoft (Instrumentos Testo S.A., Barcelona, Spain). A schematic diagram of the cooking of the crêpe is shown in Fig. 1. For color measuring, once the crêpe had cooled down, it was placed on a scanner (Canon Scan Lide 210), and the image was digitized and formatted to the CIE Lab profile to obtain the L^* coordinate.

The experimental and numerical results obtained for the average surface temperature, weight loss during cooking of a double-sided French crêpe and color evolution are represented in Fig. 10. Note that the experimental curves are discontinuous due to the turn over process. The root mean squared error of the results is 3.3 °C for the temperature, 1.16 for the weight loss and 2.12 for the luminosity parameter.

References

Aguilera, J.M., 2018. Relating food engineering to cooking and gastronomy. Compr. Rev. Food Sci. Food Saf. 17 (4), 1021–1039.

Ame, Jennifer M., 1992. Biochemistry of Food Proteins. The Maillard Reaction. Springer, US.

Bonet-Sánchez, B., Cabeza-Gil, I., Calvo, B., Grasa, J., Franco, C., Llorente, S., Martínez, M.A., 2022. A combined experimental-numerical investigation of the thermal efficiency of the vessel in domestic induction systems. Mathematics 10 (5), 802.

Cabeza-Gil, I., Calvo, B., Grasa, J., Franco, C., Llorente, S., Martínez, M., 2020a. Thermal analysis of a cooking pan with a power control induction system. Appl. Therm. Eng. 180, 115789.

Cabeza-Gil, I., Ríos-Ruiz, I., Calvo, B., 2020b. Customised selection of the haptic design in c-loop intraocular lenses based on deep learning. Ann. Biomed. Eng..

Chai, T., Draxler, R.R., 2014. Root mean square error (RMSE) or mean absolute error (MAE)? – arguments against avoiding RMSE in the literature. Geosci. Model Dev. 7 (3), 1247–1250.

Chollet, F., et al., 2015. Keras. https://github.com/fchollet/keras.

Defraeye, T., Shrivastava, C., Berry, T., Verboven, P., Onwude, D., Schudel, S., Bühlmann, A., Cronje, P., Rossi, R.M., 2021. Digital twins are coming: Will we need them in supply chains of fresh horticultural produce?. Trends Food Sci. Technol. 109, 245–258.

Dolejšová, M., Wilde, D., Bertran, F.A., Davis, H., 2020. Disrupting (more-than-) human-food interaction. In: Proceedings of the 2020 ACM Designing Interactive Systems Conference. ACM.

Kannapinn, M., Pham, M.K., Schäfer, M., 2022. Physics-based digital twins for autonomous thermal food processing: Efficient, non-intrusive reduced-order modeling. Innov. Food Sci. Emerg. Technol. 81, 103143.

Kannapinn, M., Schäfer, M., 2021. Autonomous cooking with digital twin methodology. In: 14th WCCM-ECCOMAS Congress. CIMNE.

Karadeniz, A.M., Arif, I., Kanak, A., Ergun, S., 2019. Digital twin of eGastronomic things: A case study for ice cream machines. In: 2019 IEEE International Symposium on Circuits and Systems. ISCAS, IEEE.

Kaur, M.J., Mishra, V.P., Maheshwari, P., 2019. The convergence of digital twin, IoT, and machine learning: Transforming data into action. In: Internet of Things. Springer International Publishing, pp. 3–17.

Khan, M.I.H., Sablani, S.S., Nayak, R., Gu, Y., 2022. Machine learning-based modeling in food processing applications: State of the art. Comprehensive Rev. Food Sci. Food Saf. 21 (2), 1409–1438.

Khouryieh, H.A., 2021. Novel and emerging technologies used by the U.S. food processing industry. Innov. Food Sci. Emerg. Technol. 67, 102559.

Kingma, D.P., Ba, J., 2014. Adam: A method for stochastic optimization.

Knorr, D., Augustin, M., 2021. Food processing needs, advantages and misconceptions. Trends Food Sci. Technol. 108, 103–110.

Lorente-Bailo, S., Etayo, I., Salvador, M.L., Ferrer-Mairal, A., Martínez, M.A., Calvo, B., Grasa, J., 2021. Modeling domestic pancake cooking incorporating the rheological properties of the batter, application to seven batter recipes. J. Food Eng. 291, 110261.

Mishyna, M., Chen, J., Benjamin, O., 2020. Sensory attributes of edible insects and insect-based foods – future outlooks for enhancing consumer appeal. Trends Food Sci. Technol. 95, 141–148.

Moolayil, J., 2019. Learn Keras for Deep Neural Networks. A Press.

Moya, J., Lorente-Bailo, S., Salvador, M., Ferrer-Mairal, A., Martínez, M., Calvo, B., Grasa, J., 2021. Development and validation of a computational model for steak double-sided pan cooking. J. Food Eng. 298, 110498.

Nachal, N., Moses, J.A., Karthik, P., Anandharamakrishnan, C., 2019. Applications of 3D printing in food processing. Food Eng. Rev. 11 (3), 123–141.

Ramachandran, P., Zoph, B., Le, Q.V., 2018. Searching for activation functions.

Sanz-Serrano, F., Sagues, C., Feyissa, A., Adler-Nissen, J., Llorente, S., 2017. Modeling of pancake frying with non-uniform heating source applied to domestic cookers. J. Food Eng. 195, 114–127.

Verboven, P., Defraeye, T., Datta, A.K., Nicolai, B., 2020. Digital twins of food process operations: the next step for food process models? Curr. Opin. Food Sci. 35, 79–87.

Wang, H., Sahoo, D., Liu, C., Lim, E.peng., Hoi, S.C. H., 2019. Learning cross-modal embeddings with adversarial networks for cooking recipes and food images. In: 2019 IEEE/CVF Conference on Computer Vision and Pattern Recognition. CVPR, IEEE.

Zhang, J., Kang, D., Zhang, W., Lorenzo, J.M., 2021. Recent advantage of interactions of protein-flavor in foods: Perspective of theoretical models, protein properties and extrinsic factors. Trends Food Sci. Technol. 111, 405–425.